

The CMBR and the Seeds of Galaxies

Edward L. Wright

UCLA Astronomy, PO Box 951562, Los Angeles CA 90095-1562

Abstract. The Cosmic Microwave Background Radiation (CMBR) is the radiation left over from the hot Big Bang. Its blackbody spectrum and small anisotropy provide clues about the origin and early evolution of the Universe. In particular, the spectrum of the CMBR rules out many non-gravitational models of structure formation, and the anisotropy of the CMBR provides a measure of the gravitational potential at the time of last scattering, about $10^{5.5}$ years after the Big Bang. The density inhomogeneities needed to produce the gravitational potential perturbations traced by the CMBR have grown to become the galaxies, clusters of galaxies, and superclusters that we see today.

1. Introduction

The observations made by the *COBE*¹ project (Boggess *et al.* 1992) were part of a long history of discoveries about the Universe. The replacement of Ptolemy's geocentric cosmology with the heliocentric cosmology of Copernicus was a first step in moving humanity from a unique and special position in the cosmos to a typical location. The replacement of Kapetyn's galaxy with Shapley's larger system put the Solar System quite far offcenter in the Universe. But studies of the extragalactic nebulae showed that the Universe was far larger than any one galaxy, and that the position of our Milky Way in the Universe was not unique. Hubble (1929) found a linear relationship between the distance to a galaxy and its recession velocity measured by its redshift. This observation fit in with expanding models for the Universe that had been worked out using the theory of general relativity, including the exponentially expanding but zero density de Sitter model, the critical density Einstein–de Sitter model, and the more general models found by Friedmann. The creation of the elements in Friedmann models was studied by Gamow (1946) and led to the realization that the Universe had to be hot during its early phases, and that this radiation should still be present with a current temperature of a few degrees Kelvin (Alpher & Herman (1948) compute 5 K.) But the lack of stable nuclei with $A = 5$ or $A = 8$ ultimately meant that the Gamow model for the creation of all the elements could in fact

¹ The National Aeronautics and Space Administration/Goddard Space Flight Center (NASA/GSFC) is responsible for the design, development, and operation of the Cosmic Background Explorer (COBE). Scientific guidance is provided by the COBE Science Working Group. GSFC is also responsible for the development of the analysis software and for the production of the mission data sets.

only produce hydrogen, helium and a trace of lithium (Copi, Schramm & Turner 1995). The de Sitter model was further developed by Hoyle and by Bondi & Gold into the Steady State model, in which a continuous creation of matter allowed a finite (and constant) density even though the Universe expands exponentially. And Burbidge, Burbidge, Fowler & Hoyle (1957) found that the elements heavier than helium could be made from hydrogen in stars, but later work showed that the helium to heavy element ratio produced by stars was less than the observed ratio. This “helium” problem led Dicke, Peebles, Roll & Wilkinson (1965) to search for the CMBR, but they were “scooped” by Penzias & Wilson (1965) who had seen the radiation because it was a significant contributor to the total noise in their ultra-sensitive receiver at Bell Labs. Previously Dicke, Beringer, Kyhl & Vane (1946) had placed an upper limit of < 20 K on the CMBR radiation, so it would have been easy to detect the CMBR at any time after 1945 with the microwave technology developed during WW II. Even earlier Adams (1941) calls attention to observations of interstellar CN molecules in a rotationally excited state (McKellar 1941), and this is the first observation of the CMBR. But it was only after the discovery of the CMBR by Penzias & Wilson (1965) that the rotational excitation of interstellar CN was developed into the most accurate groundbased measurement of the temperature of the CMBR, giving $T_o = 2729_{-31}^{+23}$ mK (Roth, Meyer & Hawkins 1993).

The existence of the CMBR rules out the Steady State model of the Universe, for the Universe today is not the isothermal and opaque Universe necessary to produce a blackbody spectrum. Fortunately one of the main motivations behind the Steady State – the discrepancy between the expansion age of the Universe $1/H_o$ and the measured ages of the oldest things in the Universe – has largely disappeared due to the new *HIPPARCOS* subdwarf parallaxes. These put the globular clusters further away, and hence the stars at the main sequence turnoff are more luminous and thus younger. Reid (1997) obtains an age of $t_o = 12 \pm 1$ Gyr for the oldest globular clusters. The *HIPPARCOS* recalibration of the Cepheid PL relation will probably lower the Riess, Press & Kirshner (1966) value of $H_o = 64 \pm 6$ km/sec/Mpc by a few percent, giving the dimensionless product of H_o and t_o a value of $H_o t_o = 0.76 \pm 0.1$ which is compatible with the $2/3$ predicted by the $\Omega = 1$ Einstein-de Sitter model.

The expansion of the Universe will not change the blackbody character of the CMBR. While the redshift reduces the frequency of the photons (and hence the color temperature) by a factor a , the expansion of the Universe reduces the number density of photons by a factor of a^3 , so the energy density is proportional to the color temperature to the fourth power, and a blackbody continues to look like a blackbody. Thus in the evolving Universe of the Big Bang model, if the isothermal and opaque conditions necessary to produce a blackbody exist at early times, and if there is no substantial transfer of energy into the CMBR at later times, then the spectrum of the CMBR will be very close to a blackbody, and the magnitude of the deviations can be used to determine the nature of any energy transfers into the CMBR.

The existence of the CMBR also drastically changed the theory of structure formation in the Universe. During the first few hundred thousand years after the Big Bang, photons and baryonic matter were strongly coupled by

Thompson scattering. At a time $10^{5.4}$ years² after the Big Bang, at $z \approx 1360$, the temperature has fallen to the point where helium and then hydrogen have 50% (re)combined into transparent gases⁵. The surface of last scattering ($\partial\tau/\partial\ln(1+z) = 1$) occurs later, at $z_r \approx 1160$ or $10^{5.7}$ years after the Big Bang. The electron scattering which had impeded the free motion of the CMBR photons until this epoch is removed, and the photons stream across the Universe. Before recombination, the radiation field at any point was constrained to be nearly isotropic because the rapid scattering scrambled the directions of photons. The radiation field was not required to be homogeneous, because the photons remained approximately fixed in comoving co-ordinates. After recombination, the free streaming of the photons has the effect of averaging the intensity of the microwave background over a region with a size equal to the horizon size. Thus after recombination any inhomogeneity in the microwave background spectrum is smoothed out. Note that this inhomogeneity is not lost: instead, it is converted into anisotropy. When we study the isotropy of the microwave background, we are looking back to the surface of last scattering $\approx 10^{5.5}$ years after the Big Bang. But the hot spots and cold spots we are studying existed as inhomogeneities in the Universe before recombination. Since the 7° beam used by the DMR instrument on *COBE* is larger than the horizon size at recombination, these inhomogeneities cannot be constructed in a causal fashion during the epoch before recombination in the standard Big Bang model. Instead, they must be installed “just so” in the initial conditions. In the inflationary scenario (Starobinsky 1980, Guth 1981) these large scale structures were once smaller than the horizon size during the inflationary epoch, but grew to be much larger than the horizon. Causal physics acting 10^{-35} seconds after the Big Bang can produce the large-scale inhomogeneities studied by the DMR.

A natural consequence of the inflationary scenario is the production of a perturbation spectrum which approximates the Harrison-Zel’dovich spectrum (Harrison 1970; Zel’dovich 1972; Peebles & Yu 1970). When expressed as the power spectrum of the density contrast, this give

$$P(k) = k^n \quad \text{with} \quad n = 1 \quad (1)$$

The density contrast on a length scale $\lambda = 2\pi/k$ is given by $\delta = \sqrt{k^3 P(k)}$ and is thus proportional to λ^{-2} in this model. As a result, the gravitational potential fluctuations are independent of the length scale: $\Delta\phi \propto \lambda^0$. This is known as “equal power on all scales”.

Because the density contrast of perturbations only grows in proportion to the size of the Universe, the existence of 100% density contrasts now implies the presence of 0.1% density contrasts at the epoch of recombination. Since the density of photons is proportional to T^3 , this leads to a prediction of $\Delta T/T = 3 \times 10^{-4}$ (Silk 1968). The length scale which now has $\Delta\rho/\rho = 1$ is approximately $8h^{-1}$ Mpc where $h = H_o/(100 \text{ km/sec/Mpc})$. This translates into an angle of $\theta = (800\Omega \text{ km/sec})/(2c) = 5'$. The predicted 1 mK temperature fluctuations on these scales were looked for and not seen.

However, observations of clusters of galaxies suggest that most of the matter in the Universe is non-luminous. If this *dark* matter does not emit, scatter or

² With $H_o = 50$, $\Omega = 1$.

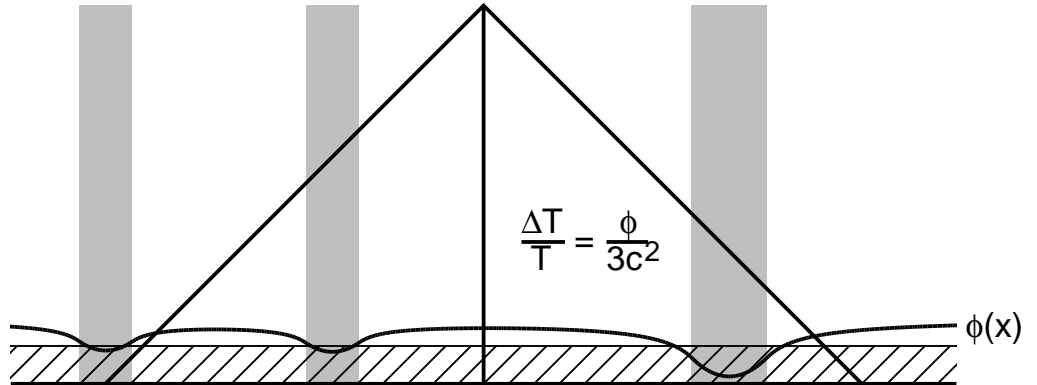


Figure 1. The Sachs-Wolfe effect produces cool spots in regions where a dense lump of matter produces a negative potential. This is a conformal space-time diagram,

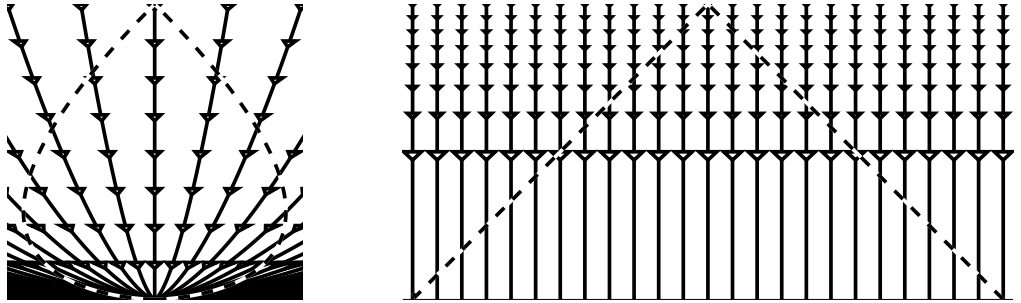


Figure 2. Comparison of an ordinary space-time diagram for an $\Omega = 1$ model on the left to a conformal space-time diagram in the right. The dashed curves are the past light cone of the central observer.

absorb light, then it will be free to collapse into gravitational potential wells while the ordinary, or *baryonic*, matter is prevented from collapsing by the radiation pressure of the CMBR. Thus the dark matter can have a density contrast of 0.1% as recombination, while the ordinary matter and photons have a much smaller density contrast. Peebles (1982) calculated the expected ΔT in this model, now called Cold Dark matter (CDM), and found tens of μK instead of 1 mK.

Another way that matter can affect the CMBR was found by Sachs & Wolfe (1967). They found that a gravitational potential perturbation produces a temperature fluctuation of $\Delta T/T = \Delta\phi/(3c^2)$. Since the potential is an integral over the density, this effect dominates at larger angular scales. Figures 1, 2 and 3 illustrate the Sachs-Wolfe effect.

2. Spectrum

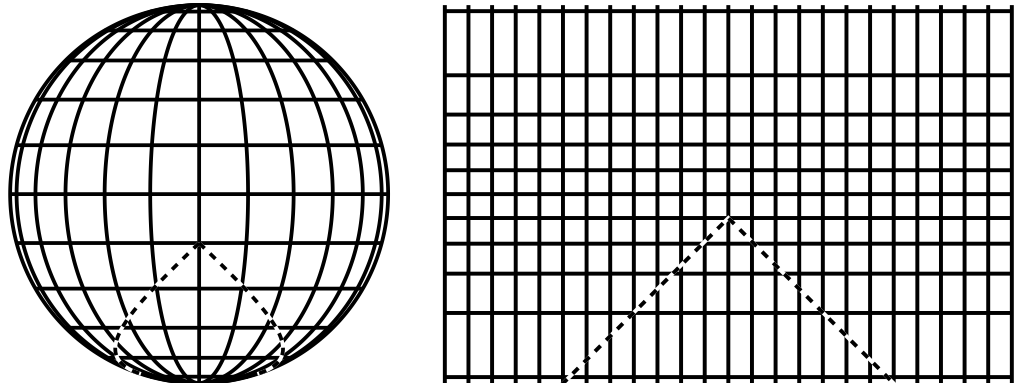


Figure 3. An analogy to Figure 2: a side view of a sphere on the left, and a conformal Mercator map on the right. The dashed curves are constant SE and SW courses.

2.1. FIRAS Observations

The Far InfraRed Absolute Spectrophotometer instrument on *COBE* is a polarizing Michelson (Martin & Puplett 1970) interferometer. The optical layout is symmetrical, and it has two inputs and two outputs. If the two inputs are denoted SKY and ICAL, then the two outputs, which are denoted LEFT and RIGHT, are given symbolically as

$$\text{LEFT} = \text{SKY} - \text{ICAL} \quad (2)$$

$$\text{RIGHT} = \text{ICAL} - \text{SKY} \quad (3)$$

The FIRAS has achieved its incredible sensitivity to small deviations from a blackbody spectrum by connecting the ICAL input to an internal calibrator, a reference blackbody that can be set to a temperature close to the temperature T_0 of the sky. Thus this “absolute” spectrophotometer is so successful because it is differential. In addition, each output is further divided by a dichroic beamsplitter into a low frequency channel ($2\text{--}21 \text{ cm}^{-1}$) and a high frequency channel ($23\text{--}95 \text{ cm}^{-1}$). Thus there are four overall outputs. These are labeled LL (left low) through RH (right high).

Since the FIRAS is a Michelson interferometer, the spectral data are obtained in the form of interferograms. Thus the LEFT output is approximately

$$I_L(x) = \int_0^\infty \cos(2\pi\nu x) G(\nu) \left(I_\nu + \sum_i \epsilon_i(\nu) B_\nu(T_i) + U_\nu \right) d\nu \quad (4)$$

The index i above runs over all the components in the FIRAS that had thermometers to measure T_i . These include the ICAL, the reference horn that connects to the ICAL, the sky horn, the bolometer housing, the optical structure of the FIRAS, and the dihedral mirrors that move to provide the variation in path length difference x . The ϵ_i 's are the effective emissivities of the various components. The ICAL itself has $\epsilon \approx -1$, while the sky and reference horns have ϵ 's of \pm a few percent in the low frequency channels. The offset term U_ν was observed

during flight to be approximately $10^{-5} \exp(-t/\tau) B_\nu(T_U)$ with a time constant τ of two months and a temperature $T_U \approx 15$ K. The SKY input I_ν above can be either the sky or an external calibrator. The XCAL is a movable re-entrant absorber that can be inserted at the top of the sky horn. The combination of sky horn plus XCAL forms a cavity with an absorptivity known to be > 0.9999 from measurements, and believed to be > 0.99999 from calculations. With the XCAL inserted during periodic calibration runs, the SKY input is known to be $B_\nu(T_X)$. By varying T_X and the other T_i 's, the calibration coefficients have been determined (Fixsen *et al.* 1994).

Once the calibration coefficients are known, the sky data can be analyzed to determine $I_\nu(l, b)$ the intensity of the sky as a function of frequency, galactic longitude and galactic latitude. This is a “data cube”. The data from each direction on the sky can be written as a combination of cosmic plus galactic signals:

$$I_\nu(l, b) = e^{-\tau_\nu(l, b, \infty)} (B_\nu(T_o + \Delta T(l, b)) + \Delta I_\nu) + \int e^{-\tau_\nu(l, b, s)} j_\nu(l, b, s) ds \quad (5)$$

where $\tau_\nu(l, b, s)$ is the optical depth between the Solar system and the point at distance s in the direction (l, b) at frequency ν , ΔI_ν is an isotropic cosmic distortion, and $\Delta T(l, b)$ is the variation of the background temperature around its mean value T_o . This equation can be simplified because the optical depth of the galactic dust emission is always small in the millimeter and sub-millimeter bands covered by FIRAS.

$$I_\nu(l, b) \approx B_\nu(T_o + \Delta T(l, b)) + \Delta I_\nu + \int j_\nu(l, b, s) ds \quad (6)$$

Even in the optically thin limit, some restrictive assumptions about the galactic emissivity j_ν are needed, since the galactic intensity $\int j_\nu(l, b, s) ds$ is a function of three variables, just like the observed data. The simplest reasonable model (Wright *et al.* 1991) for the galactic emission is

$$\int j_\nu(l, b, s) ds = G(l, b)g(\nu). \quad (7)$$

This model assumes that the shape of the galactic spectrum is independent of direction on the sky. It is reasonably successful except that the galactic center region is clearly hotter than the rest of the galaxy. The application of this model proceeds in two steps. The first step assumes that the cosmic distortions vanish, and that an approximation $g_o(\nu)$ to the galactic spectrum is known. A least squares fit over the spectrum in each pixel then gives the maps $\Delta T(l, b)$ and $G(l, b)$. The high frequency channel of FIRAS is used to derive $G(l, b)$ because the galactic emission is strongest there. An alternative way to derive $G(l, b)$ is to smooth the DIRBE map at $240 \mu\text{m}$ to the FIRAS 7° beam. A modification of this DIRBE method has been used in the latest FIRAS spectral results (Fixsen *et al.* 1996) where it is assumed that

$$\int j_\nu(l, b, s) ds = G_1(l, b)g_1(\nu) + G_2(l, b)g_2(\nu) \quad (8)$$

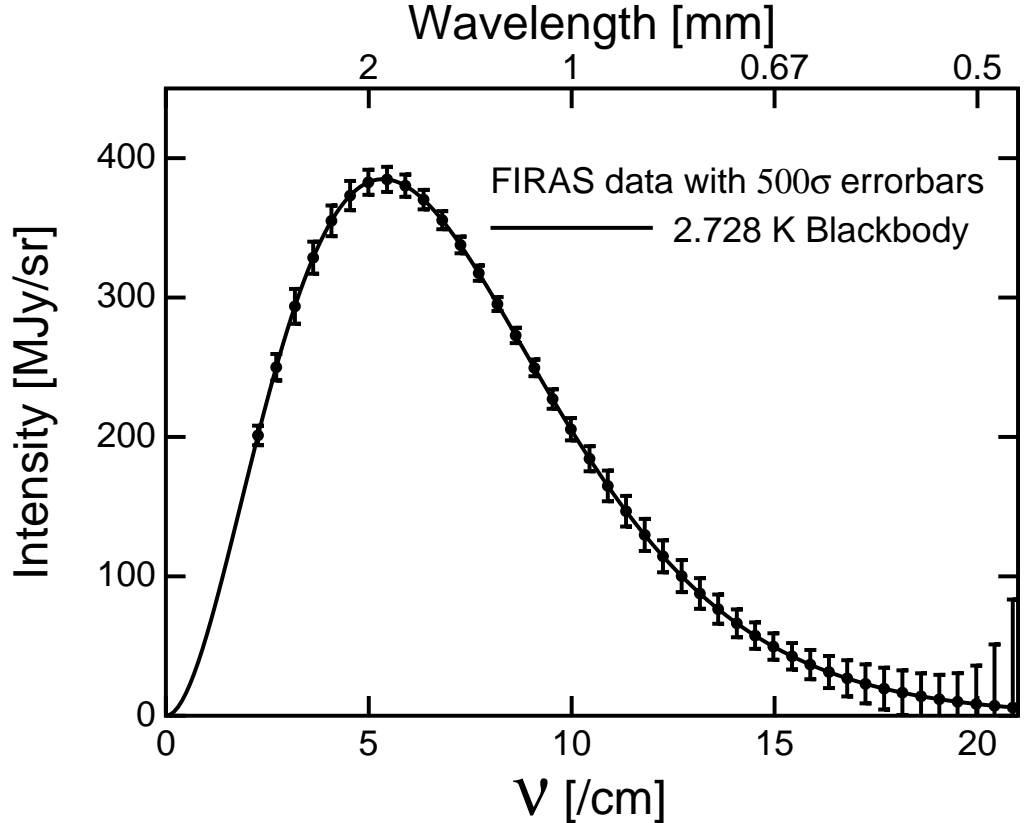


Figure 4. Spectrum of the CMBR compared to a blackbody. The error bars have been multiplied by 500 to make them visible.

and the maps G_1 and G_2 are derived from the DIRBE Band 9 (140 μm) and Band 10 (240 μm) maps.

The second step in the galactic fitting then derives spectra associated with the main components of the millimeter wave sky: the isotropic cosmic background, the dipole anisotropy, and the galactic emission(s). This fit is done by fitting all the pixels (except for the galactic center region with $|b| < 20$ and $|l| < 40$) at each frequency to the form

$$I_\nu(l, b) = I_o(\nu) + D(\nu) \cos \theta + G_1(l, b)g_1(\nu) + G_2(l, b)g_2(\nu). \quad (9)$$

The final spectrum reported for deviations of the CMBR from a blackbody is given by

$$\Delta I_\nu = I_o(\nu) - B_\nu(T_o) - G_1g_1(\nu) - G_2g_2(\nu) \quad (10)$$

where the parameters T_o , G_1 and G_2 are adjusted to minimize the χ^2 of the fit. The noise varies with frequency and noise in adjacent points is somewhat anti-correlated because of the offcenter scan used when taking the interferograms. Figure 4 shows the isotropic spectrum $I_o(\nu)$ compared to a 2.728 K blackbody.

The absolute temperature of the cosmic background, T_o , can be determined two ways using FIRAS. The first way is to use the readings of the germanium

resistance thermometers in the XCAL when the XCAL temperature is set to match the sky. This gives $T_{\circ} = 2.730$ K. The second way is to measure the frequency of the peak of $\partial B_{\nu}/\partial T$ by varying T_X a small amount around the temperature which matches the sky, and then apply the Wien displacement law to convert this frequency into a temperature. This calculation is done automatically by the calibration software, and it gives a value of 2.726 K for T_{\circ} . Three additional determinations of T_{\circ} depend on the dipole anisotropy. For either FIRAS or DMR, the spectrum of the dipole anisotropy can be fit to the form

$$D(\nu) = \frac{T_{\circ} v}{c} \frac{\partial B_{\nu}(T_{\circ})}{\partial T} \quad (11)$$

Since the velocity of the solar system with respect to the CMB is not known *a priori*, only the shape and not the amplitude of the dipole spectrum can be used to determine T_{\circ} . For FIRAS, this analysis gives $T_{\circ} = 2.717 \pm 0.007$ K (Fixsen *et al.* 1996), while for DMR it gives $T_{\circ} = 2.76 \pm 0.18$ K (Kogut *et al.* 1993). The DMR data analysis keeps track of the changes in the dipole caused by the variation of the Earth's velocity around the Sun during the year. In this case the velocity v is known, so T_{\circ} can be determined from the amplitude of the change in the dipole, giving $T_{\circ} = 2.725 \pm 0.02$ K (Kogut *et al.* 1996b). The final adopted value (Fixsen *et al.* 1996) is 2.728 ± 0.004 K (95% confidence), which just splits the difference between the two methods based on the FIRAS spectra. The dipole-based determinations of T_{\circ} are less precise but provide a useful confirmation of the spectral data.

2.2. Interpretation

For redshifts greater than $z_y = 10^{5.1}/\sqrt{70\Omega_B h^2}$, the rate of photon frequency diffusion due to Compton scattering is large:

$$(1+z) \frac{\partial y}{\partial z} = \sigma_T n_{e,\circ} \frac{kT_{\circ}}{m_e c^2} \frac{c}{H} (1+z)^4 > 1 \quad (12)$$

where the Kompaneets y is defined by $dy = (kT_e/m_e c^2) n_e \sigma_T c dt$. A Bose-Einstein distribution with dimensionless chemical potential μ , $n = 1/(\exp[x + \mu] - 1)$, is a fixed point of the Kompaneets (1957) equation:

$$\frac{\partial n}{\partial y} = x^{-2} \frac{\partial}{\partial x} \left[x^4 \left(n + n^2 + \frac{\partial n}{\partial x} \right) \right] \quad (13)$$

where n is the number of photons per mode ($n = 1/(e^x - 1)$ for a blackbody) and $x = h\nu/kT_e$. Therefore, any distortion created before z_y will be converted into a μ distortion by electron scattering. When expressed as a frequency dependent brightness temperature with a conserved photon number, the form of a μ distortion is

$$T_{\nu} = T_{\circ} \left(1 + \mu \left[\frac{\zeta(2)}{3\zeta(3)} - x^{-1} \right] + \dots \right). \quad (14)$$

This spectrum has excess energy relative to a blackbody in the amount of

$$\frac{\Delta U}{U} = \left(\frac{4\zeta(2)}{3\zeta(3)} - \frac{\zeta(3)}{\zeta(4)} \right) \mu = 0.714\mu. \quad (15)$$

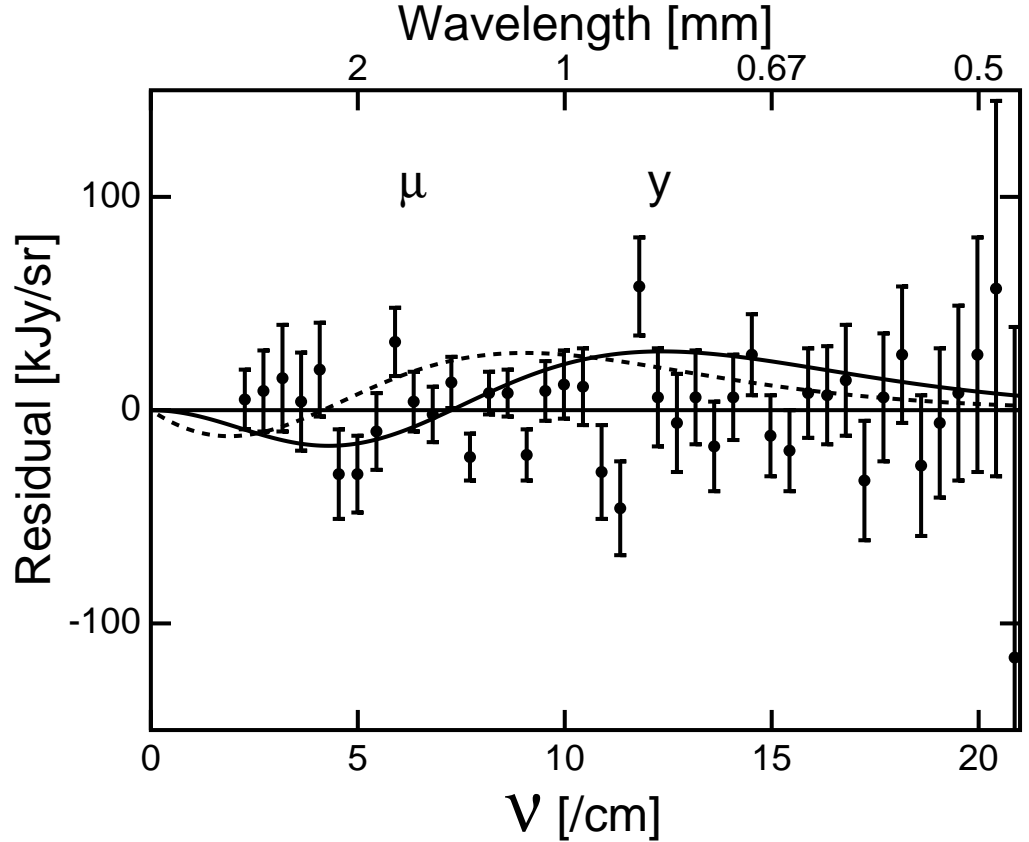


Figure 5. The residual after subtracting a blackbody and a constant times the galactic spectrum from the FIRAS CMBR spectrum. The 95% confidence limits on μ and y distortions are shown by the dashed and solid curves.

At still higher redshifts, the double photon Compton scattering process $\gamma + e^- \leftrightarrow \gamma + \gamma + e^-$ can create photons. A proper consideration (Burigana *et al.* 1991) of the interaction of this photon creation process with the Kompaneets equation shows that the redshift from which $1/e$ of an initial distortion can survive is

$$z_{th} = \frac{4.24 \times 10^5}{[\Omega_B h^2]^{0.4}} \quad (16)$$

which is $z_{th} = 2.3 \times 10^6$ for the BBNS value of $\Omega_B h^2$.

Other distortions formed at redshifts lower than z_y can survive to the present. The distortion formed when a blackbody spectrum is scattered by hotter electrons is given by a frequency-dependent temperature (Zel'dovich & Sunyaev 1969)

$$T_\nu = T_o \left[1 + y_D \left(\frac{x(e^x + 1)}{e^x - 1} - 4 \right) + \dots \right]. \quad (17)$$

where the “distorting” y is

$$dy_D = \frac{k(T_e - T_\gamma)}{m_e c^2} n_e \sigma_T c dt. \quad (18)$$

The FIRAS spectrum in Figure 5 shows that $|y_D| < 1.5 \times 10^{-5}$ and $|\mu| < 9 \times 10^{-5}$ (95% confidence), and the spectral deviations corresponding to these limits are shown by the solid and dashed curves.

The energy density transferred from the hotter electrons to the cooler photons in the y distortion is easily shown to be $\Delta U/U = 4y < 6 \times 10^{-5}$. For a μ distortion the corresponding limit is

$$\frac{\Delta U}{U} = \left(\frac{4\zeta(2)}{3\zeta(3)} - \frac{\zeta(3)}{\zeta(4)} \right) \mu = 0.714\mu < 6 \times 10^{-5}. \quad (19)$$

Thus any transfer of energy into the CMBR produced by scattering off of hot electrons is less than 60 parts per million for all redshifts less than 2×10^6 , or times later than two months after the Big Bang.

3. Anisotropy

3.1. History

The earliest predictions of $\Delta T/T$ were very large. In addition to the $\Delta T/T = 3 \times 10^{-4}$ on $5'$ scales predicted by Silk (1968), Sachs and Wolfe (1967) predicted $\Delta T/T = 1\%$ on larger angular scales based on an assumed $\Delta\rho/\rho$ of 10% over scales L such that $H_o L = 0.1c$. The Sachs-Wolfe effect predicts $\Delta T/T = (1/3)\Delta\phi/c^2$, where $\Delta\phi$ is the gravitational potential computed using Newtonian gravity produced by the density fluctuations:

$$\nabla^2(\Delta\phi) = 4\pi G\Delta\rho \quad (20)$$

The first detection of anisotropy in the CMBR (Conklin 1969) actually discovered a different effect, the dipole anisotropy with a peak amplitude of $\pm 0.12\%$ that is only indirectly related to $\Delta\rho/\rho$. By 1971 a 3σ measurement (Henry 1971) of the dipole anisotropy had been made, and its significance was discussed by Peebles (1971). The dipole anisotropy measures the velocity of the observer relative to a very large piece of the Universe: a sphere with comoving circumference $2\pi(1+z_r)D_A(z_r)$, where $D_A(z)$ is the angular size distance. This velocity is produced by the action of the gravitational acceleration $g = \vec{\nabla}(\Delta\phi)$ over the Hubble time $1/H_o$. Further observations by Smoot, Gorenstein & Muller (1977) showed no detectable deviations from the dipole pattern to a level below the expected 3×10^{-4} .

The analysis of anisotropy beyond the dipole is usually done in spherical harmonics, using

$$\frac{\Delta T(\hat{n})}{T_o} = \sum_{\ell, m} a_{\ell m} Y_{\ell m}(\hat{n}) \quad (21)$$

The rotational symmetry expected in the Universe means that all the $a_{\ell m}$'s for a given ℓ should have the same variance, and an expectation value of zero. The

variance of the $a_{\ell m}$'s is C_ℓ . For a Harrison-Zel'dovich spectrum the angular power spectrum is given by

$$C_\ell = \frac{4\pi\langle Q^2 \rangle}{5T_\odot^2} \frac{6}{\ell(\ell+1)} \quad (22)$$

The normalization is expressed in terms of $\langle Q^2 \rangle$, the expected value of the quadrupole. This is often called Q_{rms-ps} , the RMS quadrupole obtained by fitting to the power spectrum, or Q_{flat} . The amplitude expressed as δT_ℓ , which is the RMS ΔT produced by all the harmonics in a band of width $\Delta\ell = \ell$, is given by

$$\delta T_\ell = \sqrt{\frac{\ell(2\ell+1)T_\odot^2 C_\ell}{4\pi}} \approx \sqrt{2.4} Q_{flat} \quad (23)$$

Continued searches for anisotropy set upper limits to the amplitude of a Harrison-Zel'dovich spectrum of primordial density perturbations of $\sqrt{\langle Q^2 \rangle} < 55 \mu\text{K}$ in 1987 (Klypin *et al.* 1987) and $\sqrt{\langle Q^2 \rangle} < 22 \mu\text{K}$ in 1991 (Page, Cheng & Meyer 1991). The latter upper limit is only 20% higher than the eventual *COBE* detection.

3.2. DMR Observations

The Differential Microwave Radiometers (DMR) experiment on *COBE* was designed to measure small temperature differences from place to place on the sky. The DMR consists of three separate units, one for each of the three frequencies of 31.5, 53 and 90 GHz. The field of view of each unit consists of two beams that are separated by a 60° angle that is bisected by the spin axis. Each beam has a 7° FWHM. The DMR is only sensitive to the brightness difference between these two beams. This differencing is performed by a ferrite waveguide switch that connects the receiver input to one horn and then the other at a rate of 100 Hz. The signal then goes through a mixer, an IF amplifier and a video detector. The output of the video detector is demodulated by a lock-in amplifier synchronized to the input switch. The difference signal that results is telemetered to the ground every 0.5 seconds. Each radiometer has two channels: A and B. In the case of the 31.5 GHz radiometer, the two channels use a single pair of horns in opposite senses of circular polarization. In the 53 and 90 GHz radiometers there are 4 horns, and all observe the same sense of linear polarization.

A major contributor to the success of the DMR experiment was the four-fold modulation a real cosmic signal had to display: the chop at 100 Hz, the spin at 0.8 rpm, the orbital modulation at 0.01 rpm, and finally the annual variation at 1 cycle per year. Most successful anisotropy experiments have at least three-fold modulation. For example, the Saskatoon experiment (Wollack *et al.* 1997) chops with a big plate, wobbles between East and West of the North celestial pole, and looks at the daily modulation as the Earth turns. The Tenerife experiment has four-fold modulation since it chops rapidly between two horns, uses a plate to wobble, and looks at both the daily and annual modulations by tracking a given declination for a year. Thus future missions should plan to modulate the true signals from the sky in as many ways as are practical.

The major problems encountered by the DMR experiment were mainly Earth-related. The Earth's magnetic field affected the ferrite Dicke switches,

producing a false signal which could be calibrated away. The signal from the Earth’s limb, diffracted over the sunshade, was very difficult to determine as well as a potentially damaging systematic error. Thus future missions should look to observing sites well away from the Earth’s magnetic field and the Earth limb: somewhere in deep space, such as the Earth-Sun L2-halo orbit, the Earth-Moon L4 or L5 point, or a heliocentric orbit.

Wright (1996) extends the DMR sparse matrix map-making technique to “one-armed” CMBR experiments with $1/f$ noise, using the time-ordered approach developed by Wright, Hinshaw & Bennett (1996) for differential radiometers. Wright (1996) also gives more examples of systematic errors, and shows how a complicated, multiply modulated scan pattern like the DMR’s 4 way modulation can reduce the effect of systematic errors.

3.3. DMR Results

The basic DMR result is the discovery of an intrinsic anisotropy (Smoot *et al.* 1992) of the microwave background, beyond the dipole anisotropy (Conklin 1969, Lineweaver *et al.* 1996). This anisotropy, when a monopole and dipole fit to $|b| > 20^\circ$ are removed from the map, and the map is then smoothed to a resolution of $\approx 10^\circ$, is $30 \mu\text{K}$. The correlation function of this anisotropy is well fit by the expected correlation function for the Harrison-Zel’dovich spectrum of primordial density perturbations predicted by the inflationary scenario, and the amplitude ($\sqrt{\langle Q^2 \rangle} = 17 \pm 5 \mu\text{K}$ in the first year data, and $18 \pm 1.6 \mu\text{K}$ in the four year data [Bennett *et al.* 1996]) is consistent with many models of structure formation (Wright *et al.* 1992).

3.4. Galactic Interference

The emission from the galaxy shows a very strong dipole and quadrupole pattern, so removing the galactic emission is essential for accurate anisotropy measurements. The separation of the observed signals into galactic and cosmic components can be achieved using multifrequency data. The spectrum of the cosmic signal is known: $\Delta I_\nu \propto \partial B_\nu(T)/\partial T$, the spectrum of free-free emission $\Delta I_\nu \propto \nu^{-2.1}$ is known, and the synchrotron and dust components can be determined from maps at frequencies where these components dominate the spectrum.

For the DMR data, with 3 frequencies, an internal linear combination of the maps can be made that satisfies 3 criteria:

1. A cosmic signal $\rightarrow \Delta T$,
2. A free-free signal $\rightarrow 0$, and
3. The observed spectrum of the galaxy $\rightarrow 0$.

These three criteria uniquely specify the weights with which the channels maps are combined: $T_{NG} = -0.4512T_{31} + 1.2737T_{53} + 0.3125T_{90}$. Because of the high noise in the 31 GHz maps and the high coefficient for the 53 GHz maps, this combination has a noise about twice as high as the 53 + 90 maps but much less response to galactic contamination.

The DMR data can be averaged into rings of constant galactic latitude and fit to a linear function of $\csc |b|$. The slope of $59 \mu\text{K}$ per unit $\csc |b|$ in the 31

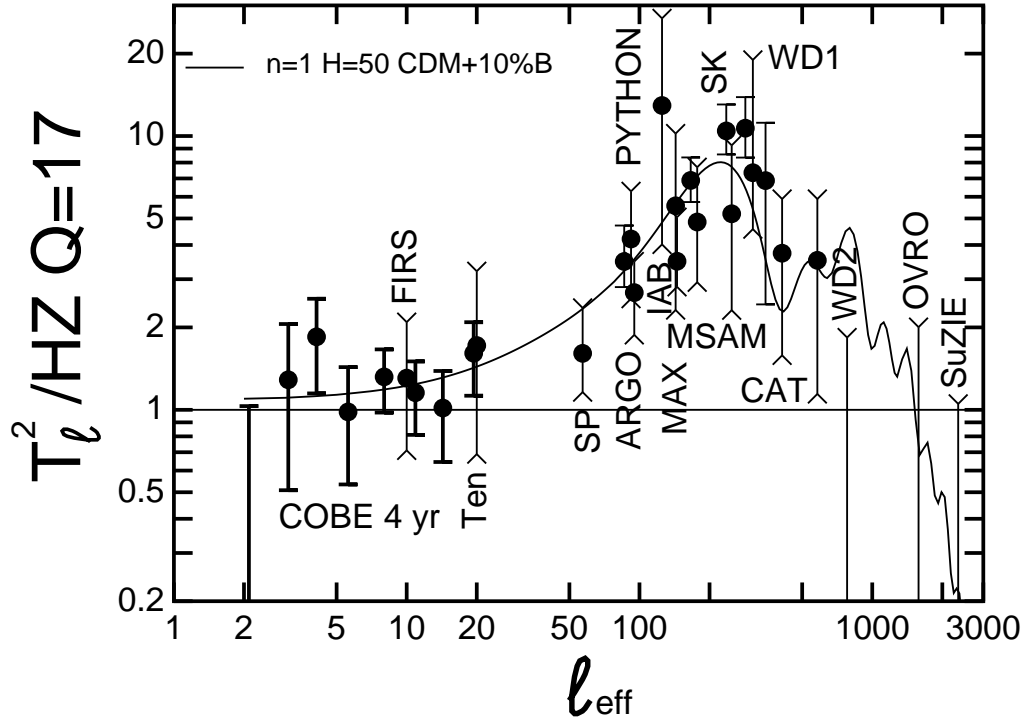


Figure 6. The angular power spectrum of the CMBR from COBE and other observations. The COBE and Saskatoon points have straight ends, while the other points have angled ends. A CDM model with $n = 1$ and $\Omega_B h^2 = 0.025$ is shown.

GHz channels is almost exactly what is expected if the slope of $17 \mu\text{K}$ per unit $\text{csc } |b|$ in the 53 GHz channels were entirely due to free-free emission. As a result this slope is zeroed out in the no galaxy (NG) maps. The slope *vs.* $\text{csc } |b|$ by itself contributes 10% of the observed variance of the 53 GHz sky smoothed to 10° resolution. This should be remembered as a cautionary note when using for the “COBE” normalization a value of $\sqrt{\langle Q^2 \rangle}$ derived from the 53 + 90 GHz maps with no attempt to remove galactic emission.

For smaller angular scales the situation improves. The dust emission has a power spectrum that follows ℓ^{-3} while the expected cosmic signal varies like ℓ^{-2} .

3.5. Power Spectrum

The power spectrum of the DMR maps has been computed by Wright *et al.* (1996) using the Hauser-Peebles method to allow for incomplete sky coverage caused by masking out the galactic plane region. Figure 6 shows the power in bands of ℓ normalized to a pure $n = 1$ (Harrison-Zel’dovich) power law with the first year amplitude $\sqrt{\langle Q^2 \rangle} = 17 \mu\text{K}$, as computed by Tegmark & Hamilton (1997) using an improved quadratic estimator that gives narrower window functions than the Hauser-Peebles method and uncorrelated errors. Also shown are results from various small and medium scale ΔT experiments: FIRS (Ganga

et al. 1994), Tenerife (Hancock *et al.* 1997), SP91 & SP94 (Gundersen *et al.* 1995), Saskatoon (Netterfield *et al.* 1997), ARGO (Masi *et al.* 1996), Python (Platt *et al.* 1997), IAB (Piccirillo & Calisse 1993), MAX (Tanaka *et al.* 1996), MSAM (Cheng *et al.* 1996), CAT (Scott *et al.* 1996), White Dish (Tucker *et al.* 1993), OVRO (Readhead *et al.* 1989), and SuZIE (Ganga *et al.* 1997). For perturbations at scales smaller than the horizon at the end of radiation dominance, dynamical effects boost the expected anisotropy. At very small scales, the finite thickness of the recombination surface filters out most of the anisotropy. The model shown in Figure 6 is a CDM model computed by Sugiyama, taken from the Berkeley CMB server, with $H_o = 50$ km/s/Mpc, $\Omega_B h^2 = 0.025$, and the $n = 1$ expected from naive inflation. The *COBE* data is consistent with the apparent spectral index n_{app} slightly greater than the $n_{pri} \lesssim 1$ that is predicted by inflation when the “toe” of the Doppler peak is included. The 2-point correlation function of the DMR data (Hinshaw *et al.* 1996a) is consistent with the power spectrum. Analysis with linear (Górski *et al.* 1996, Hinshaw *et al.* 1996b) statistics instead of the quadratic Hauser-Peebles statistics confirms this conclusion.

Note that the good agreement between the DMR correlation function or power spectrum and the Harrison-Zel’dovich model, while supporting inflation, does not prove inflation, especially since the precision with which the spectral index n can be determined is poor due to the small range of angular scales probed by *COBE*. Thus intermediate scale anisotropy data are needed for a more precise test of inflation.

The inflationary scenario also predicts that the temperature fluctuations should have a Gaussian distribution. This can be tested by looking at higher-order moments of the maps such as three point correlation functions (Kogut *et al.* 1996a), or by directly studying the probability distributions. The random measurement noise from the radiometers is still sufficient to interfere with these studies to a great extent, but a preliminary analysis finds that the Gaussian model is consistent with the observations. The three-point correlation function of the *COBE* DMR maps is consistent with the level of three-point correlation expected in a Harrison-Zel’dovich model with Gaussian fluctuations. While the expected value of the three-point correlation vanishes for Gaussian models, the variance does not, so any individual realization of the Gaussian process will have a non-zero three-point correlation function.

The CMBR field is moving so rapidly that any review article is quickly out-of-date, but White, Scott & Silk (1994) is a review of the literature on CMBR anisotropies and their interpretations up to early 1994. Remember that all of the detections on Figure 6 are less than five years old.

4. Comparison to Large Scale Structure

Wright *et al.* (1992) discussed the implications of the *COBE* DMR data for models of structure formation, and selected 4 models from a large collection given by Holtzman (1989) for detailed discussion: a “CDM” model, with $H_o = 50$ km/s/Mpc, $\Omega_{CDM} = 0.9$, and $\Omega_B = 0.1$; a mixed “CDM+HDM” model, with $H_o = 50$ km/s/Mpc, $\Omega_{CDM} = 0.6$, $\Omega_{HDM} = 0.3$ (a 7 eV neutrino), and $\Omega_B = 0.1$; an open model, with $H_o = 100$ km/s/Mpc, $\Omega_{CDM} = 0.18$, and $\Omega_B = 0.02$;

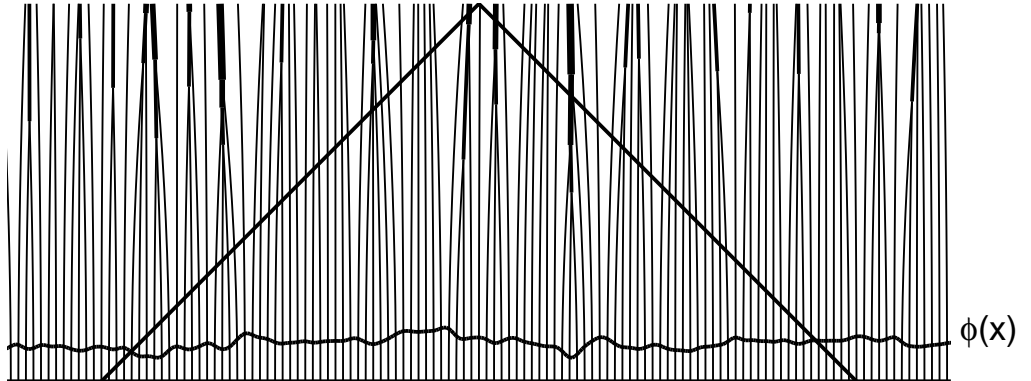


Figure 7. The potential ϕ observed using the CMBR perturbs the worldlines of galaxies in this conformal space-time diagram, producing cluster of galaxies in the “valleys” and voids in the “mountains” of the Universe.

and a vacuum dominated model, with $H_o = 100$ km/s/Mpc, $\Omega_{CDM} = 0.18$, $\Omega_B = 0.02$, and $\Omega_{vac} = 0.8$. The vacuum dominated model and especially the open model have potential perturbations now that are too small to explain the POTENT bulk flows (Bertschinger *et al.* 1990).

A comparison of the extremely large scale structure seen by *COBE*, to the large scale structure seen in studies of the clustering of galaxies also leads to an estimate of the primordial spectral index, n_{pri} . The uncertainty in this method is decreased because of the large range of scales covered, but also increased due to uncertainties in the models of large scale structure formation. However, this comparison strongly favors $n = 1$. Prior to the *COBE*, announcement of anisotropy, Peacock (1991) gave an implicit prediction that for $n = 1$ the amplitude of ΔT should be $\sqrt{\langle Q^2 \rangle} = 18.8 \mu\text{K}$. Peacock & Dodds (1994) have extended this analysis of large scale structure and I get a result $n_{pri} = 0.99 \pm 0.16$ from their paper after correcting for their incorrect $\sqrt{\langle Q^2 \rangle} = 15 \mu\text{K}$ and increasing the uncertainty to allow for the uncertainty in the IRAS bias, b_I . This result assumes that $\Omega = 1$, but Peacock & Dodds have also found that $\Omega^{0.6}/b_I = 1.0 \pm 0.2$.

So the basic question – can gravity with a strength indicated by the CMBR ΔT produce the the observed large scale structure? – has the answer: Yes – but only if most of the matter in the Universe is dark! Figure 7 shows how the CMBR gives $\phi(x)$ which then drives the matter into clusters.

5. Future CMB Work

Jungman *et al.* (1996) show that many cosmological parameters have an effect on the power spectrum of the CMB. For example, the value of Ω_o determines the location of the Doppler peak at $\ell \approx 200$ in Figure 6, while the baryon density affects its height. The position of the peak shifts to $\ell \approx 220/\sqrt{\Omega_o}$ in open models, and even today’s non-systematic collection of competing experiments shown in Figure 6 suggests that open models with $\Omega_o \approx 0.3$ can be ruled out. The nature

of the dark matter has an effect on the secondary Doppler peaks, since hot dark matter will stream out of the smaller scale structures whose “bouncing” causes the peaks. Current measurements of the small angular scale anisotropy of the CMB are limited by their small sky coverage to relatively poor precision. But a new generation of proposed experiments can improve this situation dramatically. With full sky coverage (actually only the usable 8 sr away from the galactic plane) and a small instrument beam one can achieve very high accuracy. In bins with width $\Delta\ell/\ell = 0.2$, a 1% uncertainty requires mapping at least 50,000 beam areas, which is the whole sky for scales $\geq 0.9^\circ$. Mapping the whole sky with this resolution will require a new satellite. For smaller beams, long duration balloons and observations from the South Pole will play a role along with satellites. New space missions being planned include the ESA mission *PLANCK*, formerly *COBRAS/SAMBA*, and the US mission *MAP* (Microwave Anisotropy Probe). *MAP* will have beam sizes in the $0.2 - 0.9^\circ$ range, which is 10 or more times smaller than the *COBE* DMR beam. *PLANCK* will use bolometers to observe the CMBR at shorter wavelengths and thus achieve beams sizes down to 0.07° , which is 100 times smaller than the DMR beam. If successful, these satellites will provide data with accuracy better than 1% out to $\ell > 600$ in the case of *MAP*, and out to $\ell > 2000$ in the case of *PLANCK*. New balloon experiments being planned include the US-Italian BOOMERANG mission and the US TOPHAT mission. When these precise new anisotropy measurements are obtained, they will establish several new constraints that cosmological models must satisfy.

6. Discussion

The next decade of CMBR work should be a very active one. The *MAP* satellite is under construction and should be launched in the year 2000. By 2002 data from *MAP* should tell us:

1. Whether any of the CDM dominated models with adiabatic perturbations collapsing due to gravity actually agree with the observations, and if so
2. Determine the values of the cosmological parameters H_0 , Ω_0 , Ω_B , the cosmological constant, the neutrino masses, and the amplitude and spectral index n of the primordial perturbations produced in the first picosecond after the Big Bang.

The *PLANCK* mission will be launched a few years later, but with its smaller beams and higher sensitivity it will be able to improve the determinations of cosmological parameters from about 10% accuracy down to 1% accuracy. And thus in less than one century cosmology will change from a speculative science with almost no observational data to an empirical science very tightly constrained by precise observations. These precise CMBR observations will reveal to us the nature of the seeds of galaxies.

Acknowledgments. Work at UCLA on the Microwave Anisotropy Probe is supported by NASA grant NAG53252 from the Goddard Space Flight Center.

References

- Adams, W. S. 1941, *ApJ*, 93, 11-23.
- Alpher, R. A. & Herman, R. 1948, *Nature*, 162, 774-775.
- Bennett, C. L., Banday, A. J., Górski, K. M., Hinshaw, G., Jackson, P. D., Keegstra, P., Kogut, A., Smoot, G. F., Wilkinson, D. T. & Wright, E. L. 1996, *ApJ*, 464, L1-L4.
- Bertschinger, E., Dekel, A., Faber, S. M., Dressler, A. & Burstein, D. 1990, *ApJ*, 364, 370-395.
- Boggess, N. et al. 1992, *ApJ*, 397, 420-429.
- Burbidge, E. M., Burbidge, G. R., Fowler, W. A. & Hoyle, F. 1957, *Rev.Mod.Phys.*, 29, 547-650.
- Burigana, C., De Zotti, G. F., & Danese, L. 1991, *ApJ*, 379, 1-5.
- Cheng, E., Cottingham, D., Fixsen, D., Inman, C., Kowitt, M., Meyer, S., Page, L., Puchalla, J., Ruhl, J. & Silverberg, R. 1996, *ApJ*, L71.
- Conklin, E. K. 1969, *Nature*, 222, 971-972.
- Copi, C., Schramm D. & Turner, M. 1995, *Science*, 267, 192-199.
- Dicke, R. H., Beringer, R., Kyhl, R. & Vane, A. B. 1946, *Phys.Rev.*, 70, 340-348.
- Dicke, R. H., Peebles, P. J. E., Roll, P. G., & Wilkinson, D. T. 1965, *ApJ*, 142, 414-419.
- Fixsen, D. J., Cheng, E. S., Gales, J. M., Mather, J. C., Shafer, R. A. & Wright E. L. 1996, *ApJ*, 473, 576-587.
- Fixsen, D. J., Cheng, E. S., Cottingham, D. A., Eplee, R. E., Jr., Hewagama, T., Isaacman, R. B., Jensen, K. A., Mather, J. C., Massa, D. L., Meyer, S. S., Noerdlinger, P. D., Read, S. M., Rosen, L. P., Shafer, R. A., Trenholme, A. R., Weiss, R., Bennett, C. L., Boggess, N. W., Wilkinson, D. T. & Wright, E. L. 1994, *ApJ*, 420, 457-473.
- Gamow, G. 1946, *Phys.Rev.*, 70, 572-573.
- Ganga, K., Page, L., Cheng, E. & Meyer, S. 1994, *ApJ*, 432, L15-L18.
- Ganga, K., Ratra, B., Church, S., Sugiyama, N., Ade, P., Holzappel, W. Lange, A. & Mauskopf, P. 1997, *ApJ* in press (astro-ph/9702186)
- Górski, K., Banday, A., Bennett, C., Hinshaw, G., Kogut, A., Smoot, G., Wright, E. 1996, *ApJ*, 464, L11.
- Gundersen, J. O., Lim, M., Staren, J., Wuensche, C. A., Figueiredo, N., Gaier, T. C., Koch, T., Meinhold, P. R., Seiffert, M. D., Cook, G., Segale, A. & Lubin, P. M. 1995, *ApJ*, 443, L57.
- Guth, A. 1981, *Phys.Rev.D*, 23, 347.
- Hancock, S., Gutierrez, C., Davies, R., Lasenby, A., Rocha, G., Rebolo, R., Watson, R. & Tegmark, M. 1997, *MNRAS* in press.
- Harrison, E. R. 1970, *Phys.Rev.D*, 1, 2726-2730.
- Henry, P. S. 1971, *Nature*, 231, 516.
- Hinshaw, G., Banday, A., Bennett, C., Górski, K., Kogut, A., Lineweaver, C., Smoot, G. & Wright, E. 1996a, *ApJ*, 464, L25.

- Hinshaw, G., Banday, A., Bennett, C., Górski, K., Kogut, A., Smoot, G. & Wright, E. 1996b ApJ, 464, L17.
- Holtzman, Jon A. 1989, ApJS, 71, 1-24.
- Hubble, E. 1929, PNAS, 15, 168-173.
- Jungman, G., Kamionkowski, M., Kosowsky, A. & Spergel, D. 1996, Phys.Rev.Lett, 76, 1007-1010.
- Klypin, A. A., Sazhin, M. V., Strukov, I. A., & Skulachev, D. P. 1987, Sov. Astr. Letters, 13, 104-107.
- Kogut, A., Lineweaver, C., Smoot, G. F., Bennett, C. L., Banday, A., Boggess, N. W., Cheng, E. S., De Amici, G., Fixsen, D. J., Hinshaw, G., Jackson, P. D., Janssen, M., Keegstra, P., Loewenstein, K., Lubin, P., Mather, J. C., Tenorio, L., Weiss, R., Wilkinson, D. T., & Wright, E. L. 1993, ApJ, 419, 1.
- Kogut, A., Banday, A., Bennett, C., Górski, K., Hinshaw, G., Smoot, G. & Wright E. 1996a, ApJ, 464, L29.
- Kogut, A., Banday, A., Bennett, C., Górski, K., Hinshaw, G., Jackson, P., Keegstra, P., Lineweaver, C., Smoot, G., Tenorio, L. & Wright, E. 1996b, ApJ, 470, 653-673.
- Kompaneets, A. S. 1957, Sov. Phys. JETP, 4, 730.
- Lineweaver, C., Tenorio, L., Smoot, G., Keegstra, P., Banday, A. & Lubin, P. 1996, ApJ, 470, 38.
- Martin, D. H. & Puplett, E. 1970, Infrared Physics, 10, 105-109.
- McKellar, A. 1941 Publ.Dom.Astr.Obs., (Victoria, BC), 7, 251.
- Masi, S., de Bernardis, P., de Petris, M., Gervasi, M., Boscaleri, A., Aquilini, E., Martinis, L. & Scaramuzzi, F. 1996, ApJ, 463, L47.
- Netterfield, C. B., Devlin, M. J., Jarosik, N., Page, L. & Wollack, E. J. 1997, ApJ, 474, 47-66.
- Page, L. A., Cheng, E. S. & Meyer, S. S. 1991, BAAS, 23, 1399.
- Peacock, J. A. 1991, MNRAS, 253, 1p-5p.
- Peacock, J. A. & Dodds, S. J. 1994, MNRAS, 267, 1020-1034.
- Peebles, P. J. E. & Yu, J. T. 1970, ApJ, 162, 815-836.
- Peebles, P. J. E. 1971, *Physical Cosmology*, (Princeton: Princeton University Press).
- Peebles, P. J. E 1982, ApJ, 263, L1-L5.
- Penzias, A. A. & Wilson, R. W. 1965, ApJ, 142, 419-421.
- Piccirillo, L. & Calisse, P. 1993, ApJ, 411, 529-533.
- Platt, S. R., Kovac, J., Dragovan, M., Peterson, J. B. & Ruhl, J. E. 1997, ApJ, 475, L1-L4.
- Readhead, A. C. S., Lawrence, C. R., Myers, S. T., Sargent, W., Hardebeck, H. E. & Moffet, A. T. 1989, ApJ, 346, 566.
- Reid, I. N. 1997, AJ, 114, 161-179.
- Riess, A., Press, W. & Kirshner, R. 1996, ApJ, 473, 88.
- Roth, K. C., Meyer, D. M. & Hawkins, I. 1993, ApJ, 413, L67.

- Sachs, R. K. & Wolfe, A. M. 1967, ApJ, 147, 73.
- Scott, P. F., Saunders, R., Pooley, G., O'Sullivan, Cr  idhe, Lasenby, A. N., Jones, M., Hobson, M. P., Duffett-Smith, P. J. & Baker, J. 1996, ApJ, 461, L1-L4.
- Silk, J. 1968, ApJ, 151, 459-471.
- Smoot, G. F., Gorenstein, M. V. & Muller, R. A. 1977, Phys.Rev.Lett, 39, 898.
- Smoot, G. F. *et al.* 1992, ApJ, 396, L1,
- Starobinsky, A. A. 1980, Physics Letters B, 91B, 99-102.
- Tanaka, S. T., Clapp, A., Devlin, M., Figueiredo, N., Gundersen, J., Hanany, S., Hristov, V., Lange, A., Lim, M., Lubin, P., Meinhold, P., Richards, P., Smoot, G., & Staren, J. 1996, ApJ, 468, L1.
- Tegmark, M. & Hamilton, A. 1997, astro-ph/9702019
- Tucker, G. S., Griffin, G. S., Nguyen, H. T. & Peterson, J. B. 1993, ApJ, 419, L45.
- White, M., Scott, D. & Silk, J. 1994, ARA&A, 32, 319-370.
- Wollack, E., Devlin, M., Jarosik, N., Netterfield, C., Page, L. & Wilkinson, D. 1997, ApJ, 476, 440.
- Wright, E. L. 1996, astro-ph/9612007
- Wright, E. L., Hinshaw, G. & Bennett, C. 1996, ApJ, 458, L53-L56
- Wright, E. L., Mather, J. C., Bennett, C. L., Cheng, E. S., Shafer, R. A., Fixsen, D. J., Eplee, R. E. Jr., Isaacman, R. B., Read, S. M., Boggess, N. W., Gulkis, S. G., Hauser, M. G., Janssen, M., Kelsall, T., Lubin, P. M., Meyer, S. S., Moseley, S. H. Jr., Murdock, T. L., Silverberg, R. F., Smoot, G. F., Weiss, R., and Wilkinson, D. T., 1991, ApJ, 381, 200-209.
- Wright, E. L. *et al.* 1992, ApJ, 396, L13.
- Zel'dovich, Ya. B. & Sunyaev, R. A. 1969, Ap&SS, 4, 301-316.
- Zel'dovich, Ya. B. 1972, MNRAS, 160, 1p.